catalysts

MDPI

Supplementary Materials

Insight into Composition and Intermediate Evolutions of Copper-Based Catalysts during Gas-Phase CO_2 Electroreduction to Multicarbon Oxygenates

Guihua Li [1,2], Yonghui Zhao [1], Jerry Pui Ho Li [3], Wei Chen [1,2,*], Shoujie Li [1], Xiao Dong [1], Yanfang Song [1], Yong Yang[3,*], Wei Wei [2,3,*] and Yuhan Sun [2,3,*]

[1] CAS Key Laboratory of Low-carbon Conversion Science and Engineering, Shanghai Advanced Research Institute, Chinese Academy of Sciences, Shanghai 201210, China; liguihua@sari.ac.cn (G.L.); zhaoyh@sari.ac.cn (Y.Z.); lishoujie@sari.ac.cn (J.L.); dongxiao@sari.ac.cn (X.D.); songyf@sari.ac.cn (Y.S.)

[2] University of the Chinese Academy of Sciences, Beijing 100049, China

[3] School of Science and Technology, ShanghaiTech University, Shanghai 201210, China jerryli_@hotmail.com (J.L.)

* Correspondence: chenw@sari.ac.cn (W.C.); yangyong@shanghaitech.edu.cn (Y.Y.); weiwei@sari.ac.cn (W.W.); sunyh@sari.ac.cn (Y.S.); Tel.: +86-21-20350954 (W.C.); +86-21-20608005 (Y.S.); Fax: +86-21-20350867 (W.C.); +86-21-20350867 (Y.S.)

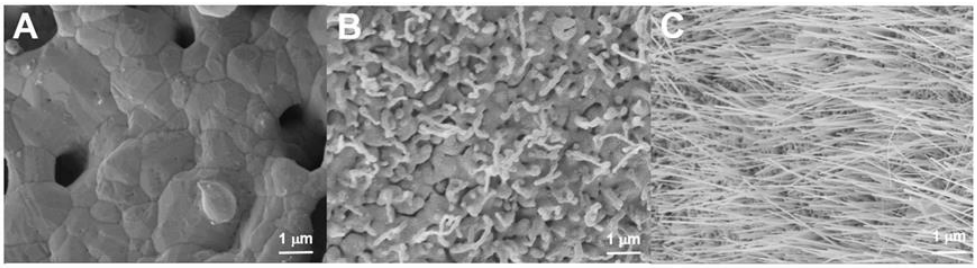

Figure S1. SEM images of (A) Cu foam, (B) Cu_2O NWs, and (C) CuO NWs.

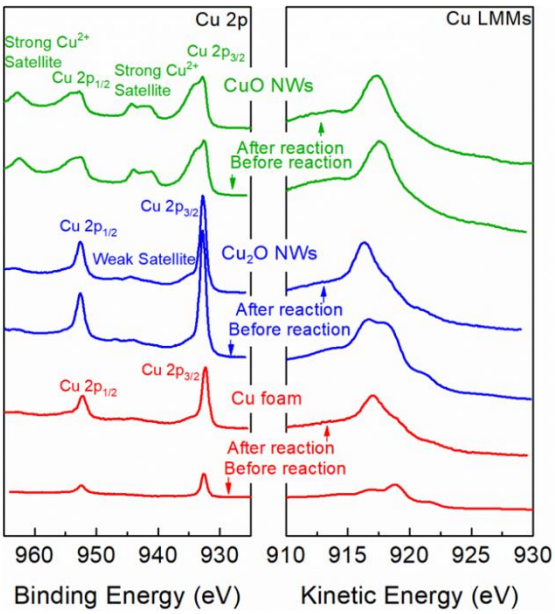

Figure S2. Cu 2p and Cu LMMs spectra of Cu-based catalysts: Cu foam, Cu_2O NWs and CuO NWs before and after one-hour gas-phase CO_2 electroreduction.

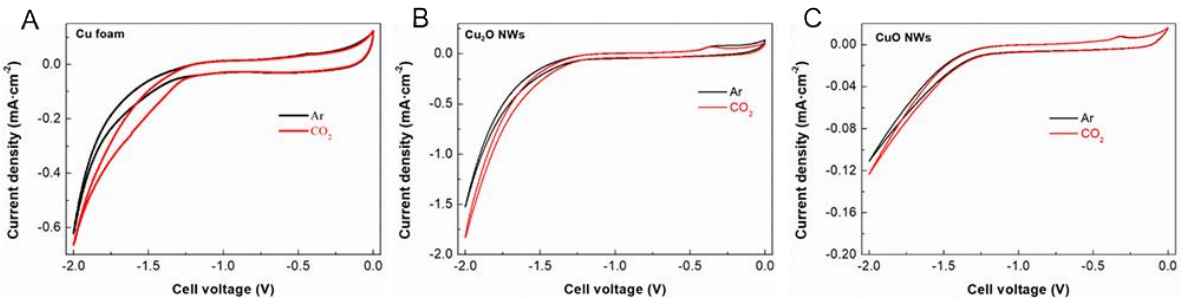

Figure S3. CV curves of (A) Cu foam, (B) Cu_2O NWs and (C) CuO NWs in Ar and CO_2 atmosphere saturated with water vapor in the cell voltage range from 0 V to -2.0 V.

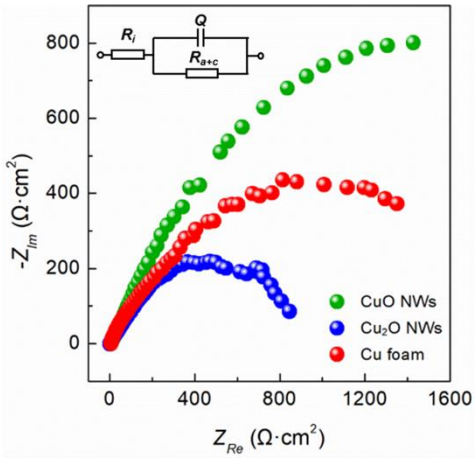

Figure S4. EIS spectra of Cu foam, Cu_2O NWs and CuO NWs in water vapor-saturated CO_2. Inset: the corresponding equivalent circuit.

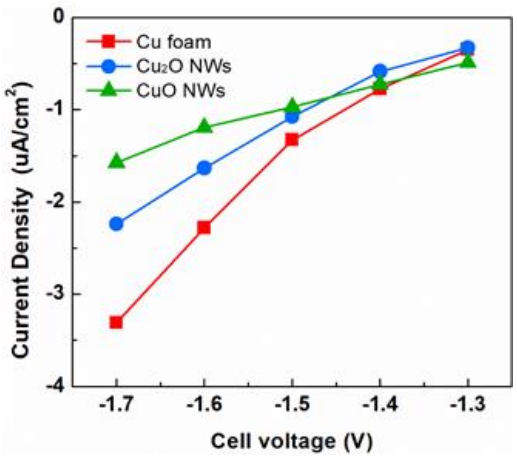

Figure S5. Current densities of gas-phase CO_2 electroreduction over Cu-based catalysts (Cu foam, Cu_2O NWs and CuO NWs) at the different cell voltages in the range of -1.3 V to -1.7 V.

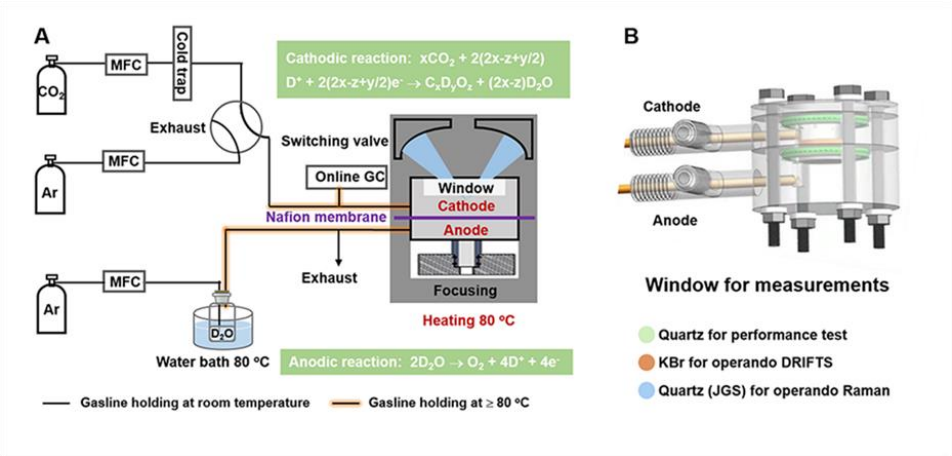

Figure S6. (A) Illustration of operando DRIFTS and Raman measurements system and (B) Home-made H-cell reactor of gas-phase CO_2 electroreduction and operando characterizations. (performance test with quartz, operando DRIFTS with KBr window and operando Raman with quartz window, respectively).

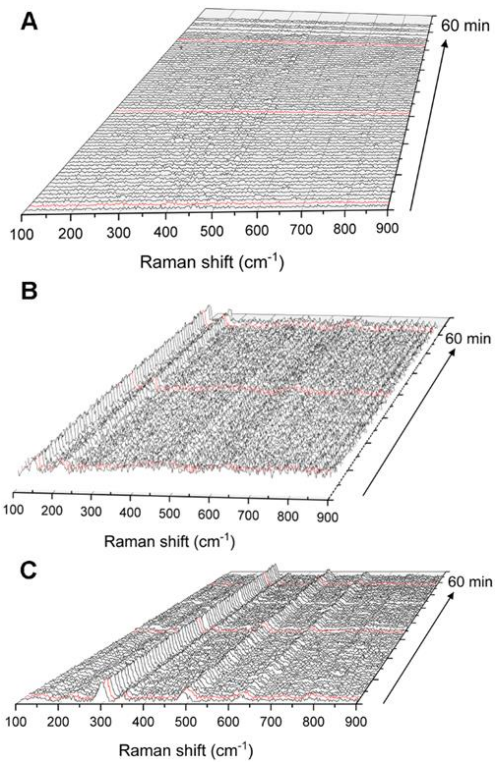

Figure S7. Operando Raman spectra of (A) Cu foam, (B) Cu_2O NWs and (C) CuO NWs for CO_2 electroreduction at -1.6 V for 1 h, respectively.

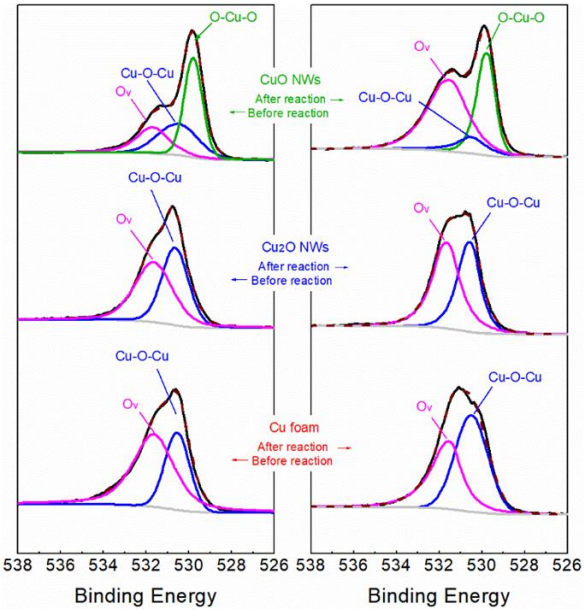

Figure S8. O 1s spectra of Cu-based catalysts: Cu foam, Cu_2O NWs and CuO NWs before and after one-hour gas-phase CO_2 electroreduction.

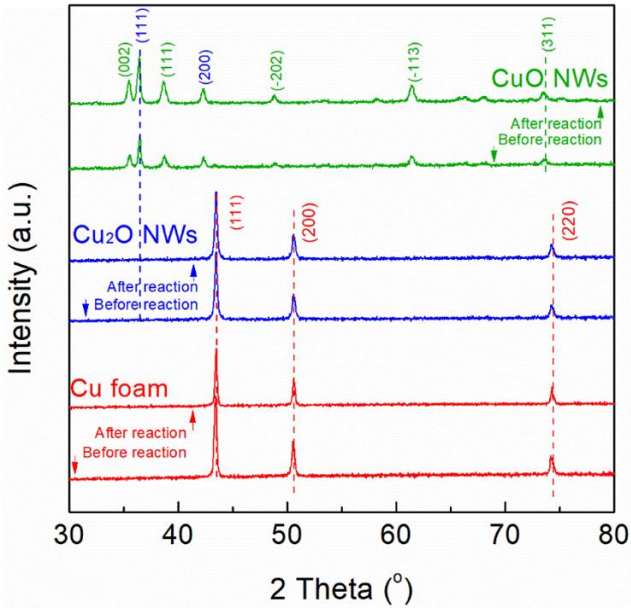

Figure S9. XRD patterns of Cu-based catalysts: Cu foam, Cu_2O NWs and CuO NWs before and after one-hour gas-phase CO_2 electroreduction.

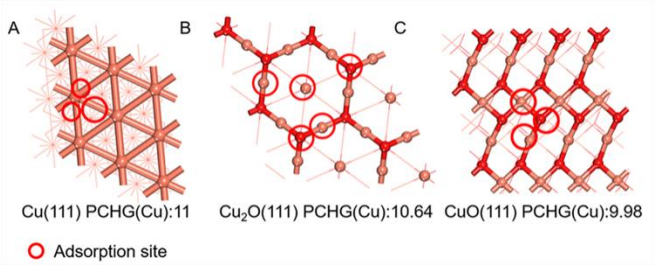

Figure S10. Surface-structure models of (A) Cu (111), (B) Cu_2O (111), and (C) CuO (111) surfaces, respectively.

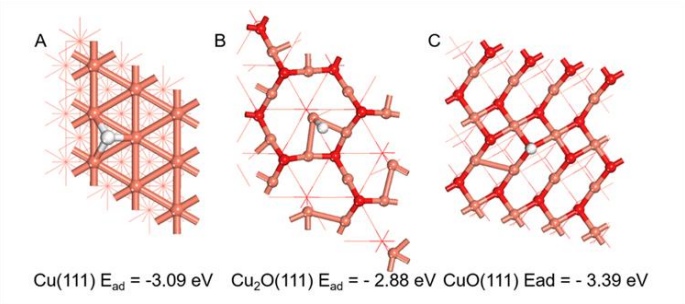

Figure S11. Relative adsorption energy of H* on (A) Cu (111), (B) Cu_2O (111), and (C) CuO (111) surfaces, respectively.

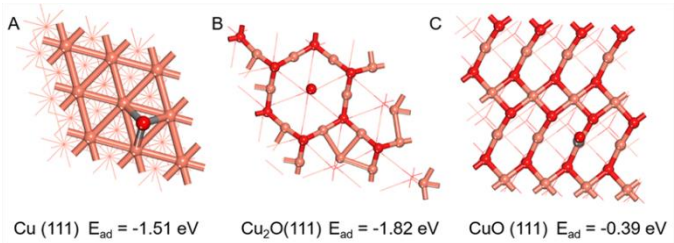

Figure S12. Relative adsorption energy of *CO on (A) Cu (111), (B) Cu_2O (111), and (C) CuO (111) surfaces, respectively.

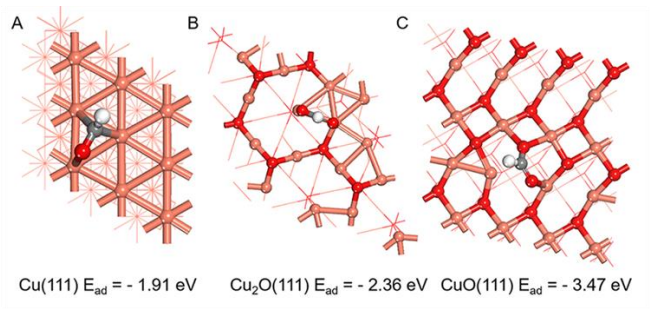

Figure S13. Relative adsorption energy of HCO* on (A) Cu (111), (B) Cu_2O (111), and (C) CuO (111) surfaces, respectively.

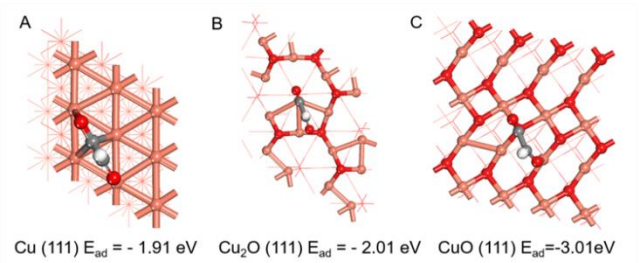

Figure S14. Relative adsorption energy of COCHO on (A) Cu (111), (B) Cu_2O (111), and (C) CuO (111) surfaces, respectively.

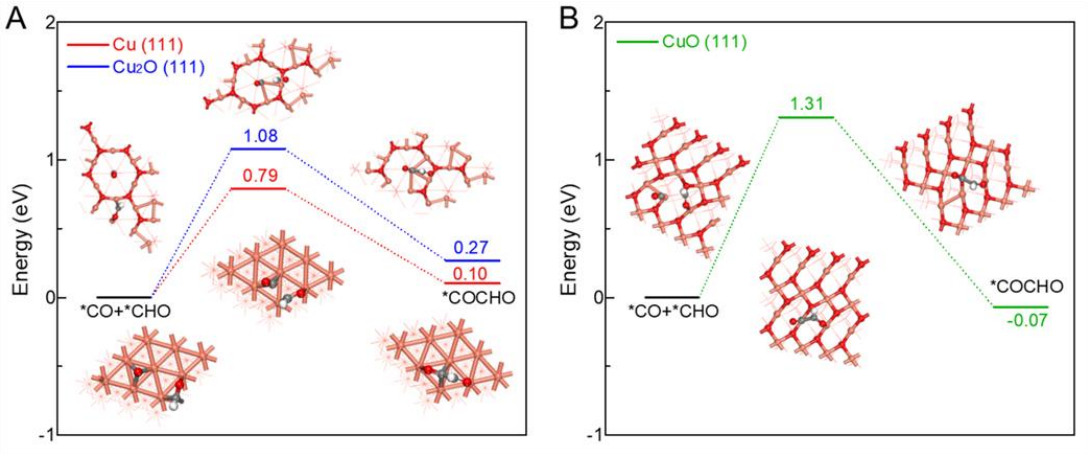

Figure S15. Activation barriers and reaction energies of CO* + HCO* → COCHO* on (A) Cu (111) surface and Cu_2O(111), respectivley, and (B) CuO(111) surface.

© 2021 by the authors. Submitted for possible open access publication under the terms and conditions of the Creative Commons Attribution (CC BY) license (http://creativecommons.org/licenses/by/4.0/).